A New Algorithm for Local Blur-Scale Computation and Edge Detection

Indranil Guha[1] and Punam K. Saha[1]

[1] University of Iowa, Electrical and Computer Engineering, Iowa City, IA, 52242, USA
indranil-guha@uiowa.edu
pksaha@healthcare.uiowa.edu

Abstract. Precise and efficient object boundary detection is the key for successful accomplishment of many imaging applications involving object segmentation or recognition. Blur-scale at a given image location represents the transition-width of the local object interface. Hence, the knowledge of blur-scale is crucial for accurate edge detection and object segmentation. In this paper, we present new theory and algorithms for computing local blur-scales and apply it for scale-based gradient computation and edge detection. The new blur-scale computation method is based on our observation that gradients inside a blur-scale region follow a Gaussian distribution with non-zero mean. New statistical criteria using maximal likelihood functions are established and applied for local blur-scale computation. Gradient vectors over a blur-scale region are summed to enhance gradients at blurred object interfaces while leaving gradients at sharp transitions unaffected. Finally, a blur-scale based non-maxima suppression method is developed for edge detection. The method has been applied to both natural and phantom images. Experimental results show that computed blur-scales capture true blur extents at individual image locations. Also, the new scale-based gradient computation and edge detection algorithms successfully detect gradients and edges, especially at the blurred object interfaces.

Keywords: Scale, intensity gradient, blur-scale, maximum likelihood function, Mahalanobis distance, edge detection.

1 Introduction

Computerized image analysis and understanding [1, 2] has drawn major attention over the last two decades inspired by the rapid growth in image data generated from different sections of human society including medical imaging and social networking. Object segmentation, quantitative structural analysis, and recognition are key challenges in many imaging applications. [3-8] The performance of most object segmentation methods is largely dependent on accurate definition and detection of object interfaces and edges. [9, 10] Often, object interfaces or boundaries are defined by sudden or gradual shifts in single or multiple image properties. For example, in a grayscale image, object interfaces are distinguished by changes in image intensity

values.[11] Such shifts in image properties at object interfaces may be sudden or gradual, and the notion of blur-scale [10, 12] is used to express transition-widths of object interfaces. Blur-scales may be different for different images; also, it may be space-variant within the same image.

In general, image segmentation algorithms [13-20] use high intensity gradients to define object boundaries. However, difficulties emerge at object interfaces with large blur-scales, where intensity changes from one object to the other are gradual, and a condition of high intensity gradients may fail causing leakages. Thus, it is essential to determine blur-scales to capture the total intensity shift across a full transition of intensities between two objects for accurate and robust detection of edges. Several theories and methods have been proposed in the literature to compute space-variant blur-scales and their applications for edge detection. [9, 12] To the best of our knowledge, Marr and Hildreth [12] first introduced the notion of blur-scale and used the second derivative of multi-scale Gaussian kernels and zero crossing segments of different scales for edge detection. Canny [9] presented a multi-scale edge detection algorithm using novel approaches of non-maximal suppression generating single pixel thick edges and hysteresis allowing two threshold values for improved discrimination among noisy and true edge segments. Canny's edge detection algorithm has been widely used, and it has been further studied and improved by others. Bao *et al*. [21] improved Canny's method and suggested to combine gradient responses at different scales by multiplication and use the combined gradient response for edge detection. Bergholm [22], proposed an edge detection algorithm that tracks events important to edge detection from the coarse to finer scale to localize the edges accurately. There are several methods in the literature, which explicitly compute local blur-scales. [10, 23, 24] Jeong and Kim [23] developed an adaptive scale based edge detection algorithm where local optimum scale is defined by the size of the Gaussian filter that minimizes a predefined energy function. As reported by the authors, the scale computation results are sensitive to local minima issues of the energy function. Lindeberg [24] presented a similar local scale computation algorithm for edge detection, where optimal scale at a pixel is determined at the maxima of a local edge strength function. Elder and Zucker [10] proposed a local blur-scale computation based edge detection algorithm, where the intensity profile across an object transition is modeled using a pre-defined sigmoid function.

Most of the above algorithms use a pre-defined model for edge transition functions and suffer from local optima related problems. In this paper, we present a model-independent local blur-scale computation algorithm and apply it for edge detection. Our method is based on a simple observation that intensity gradients over a blur-scale region follow a Gaussian distribution with a non-zero mean. A blur-scale based gradient computation method has been presented that enhances gradients at blurred edges while leaving gradients at sharp edges unaffected. Finally, a scale-based edge detection algorithm is developed using scale-based gradients.

2 Theory and Algorithms

In this section, we describe new theory and algorithms to compute local blur-scale and present its application to edge detection. In general, in a true scene, object interfaces form sharp transition in illumination or material density. Finite image resolution or other artifacts, add blur at such interfaces. Specifically, in a grayscale image, blur-scale of an object interface at a given location is the transition-width of the interface at that location. The premise of our blur-scale computation algorithm is based on a simple observation that intensity gradients inside a local blur-scale region follow a Gaussian distribution with nonzero mean. In the following paragraphs, we formulate new test criteria and present a new algorithm for blur-scale computation guided by this observation, and finally describe its application in edge detection.

Let I denote an image intensity function and $\nabla\mathbf{x}_i$ denote the gradient vector at a given location $\mathbf{x}_i$. The blur-scale computation algorithm is developed based on the evaluation of two hypotheses. Our first hypothesis is that observed gradient vectors $\nabla\mathbf{x}_1, \nabla\mathbf{x}_2, \cdots, \nabla\mathbf{x}_n$ inside a blur-scale region are random samples from a population with an expected probability density function (pdf) $G(\cdot\,|\boldsymbol{\mu}_\mathrm{e}, \Sigma_\mathrm{e})$, where $\boldsymbol{\mu}_\mathrm{e}$ and Σ_e are the mean and covariance matrix of gradient vectors. Let X_o denote the set $\{\nabla\mathbf{x}_1, \nabla\mathbf{x}_2, \cdots, \nabla\mathbf{x}_n\}$. We formulate a test criterion to evaluate the first hypothesis based on the ratio of two likelihood estimators. [25] Let $\mathcal{P}_n$ denote the set of all possible sets of n gradient vectors. Let $L(\boldsymbol{\mu}_\mathrm{e}, \Sigma_\mathrm{e}|X)$ denote the likelihood measure that the gradient vectors in a set $X \in \mathcal{P}_n$ are random samples from a population with the pdf $G(\cdot\,|\boldsymbol{\mu}_\mathrm{e}, \Sigma_\mathrm{e})$. Thus, the following likelihood ratio estimator evaluates whether gradient vectors in X_o are random samples from a known population:

$$\lambda_1(X_\mathrm{o}|\boldsymbol{\mu}_\mathrm{e}, \Sigma_\mathrm{e}) = \frac{L(\boldsymbol{\mu}_\mathrm{e}, \Sigma_\mathrm{e}|X_\mathrm{o})}{\sup\limits_{X\in\mathcal{P}_n} L(\boldsymbol{\mu}_\mathrm{e}, \Sigma_\mathrm{e}|X)}\ . \tag{1}$$

To test our hypothesis, we define a rejection region of the form $\lambda_1(X_\mathrm{o}|\boldsymbol{\mu}_\mathrm{e}, \Sigma_\mathrm{e}) \le c_1$, where $c_1 \mid 0 \le c_1 \le 1$ is the rejection confidence. Using the fact that the largest value of $L(\boldsymbol{\mu}_\mathrm{e}, \Sigma_\mathrm{e}|X)$ occurs when all gradient vectors in X equates to $\boldsymbol{\mu}_\mathrm{e}$, it can be shown that $\lambda_1(X_\mathrm{o}|\boldsymbol{\mu}_\mathrm{e}, \Sigma_\mathrm{e}) \le c_1$is equivalent to the following test criterion:

$$\sqrt{\frac{\sum_{i=1}^{n} d_M^2(\nabla\mathbf{x}_i, \boldsymbol{\mu}_\mathrm{e}, \Sigma_\mathrm{e})}{n}} > \sqrt{\frac{-2\log c_1}{n}}, \tag{2}$$

where $d_M(\nabla\mathbf{x}_i, \boldsymbol{\mu}_\mathrm{e}, \Sigma_\mathrm{e})$ is the Mahalanobis distance [26] of $\mathbf{x}_i$ from the mean $\boldsymbol{\mu}_\mathrm{e}$ using the covariance matrix Σ_e.

Our second hypothesis is that the mean of the gradient vectors $\nabla\mathbf{x}_1, \nabla\mathbf{x}_2, \cdots, \nabla\mathbf{x}_n$ is non-zero. In other words, we examine whether the Mahalanobis distances from the set $D_\mathrm{o} = \{d_M(\nabla\mathbf{x}_i, \mathbf{0}, \Sigma_\mathrm{N}) | i = 1 \text{ to } n\}$ are random samples from a standard normal distribution, where Σ_N represents image noise derived from homogeneous regions. Note that $d_M(\nabla\mathbf{x}_i, \mathbf{0}, \Sigma_\mathrm{N})$ is the Mahalanobis distance of a gradient vector $\nabla\mathbf{x}_i$ from

the null vector $\mathbf{0}$. Hence, the rejection region for the second hypothesis is formulated as:

$$\lambda_2(D_o) = \frac{L(0,1|D_o)}{\sup_{\mu} L(\mu,1|D_o)} \leq c_2, \tag{3}$$

where $c_2 \mid 0 \leq c_2 \leq 1$ is the rejection confidence. It can be shown that the maximum value of the likelihood estimation $L(\mu,1|D_o)$ happens when μ equates to the mean μ_o of Mahalanobis distances in D_o. Using the optimality criterion and a few algebraic operations, we can rewrite (3) as follows:

$$\frac{\sum_{i=1}^{n} d_M(\nabla \mathbf{x}_i, \mathbf{0}, \Sigma_N)}{n} > \sqrt{\frac{-2\log c_2}{n}}. \tag{4}$$

2.1 Algorithms

The new blur-scale computation algorithm starts with the computation of gradient vectors at all image pixels using a derivative of Gaussian (DoG) kernel. The method computes the blur-scale at each image pixel using a star line approach and an iterative method. A blur-scale region at a pixel p is a circular disk centered at p, and its diameter $2r$ represents the corresponding blur-scale. At a given pixel, the scale computation starts with $r = 0.5$, and after each iteration, the value of r is incremented by 0.5 until both hypotheses are rejected or a maximum scale value occurs. At a given pixel p and a scale $2r$, we verify the test criteria defined in Equations (2) and (4) as follows. First, we compute the set $X_o = \{\nabla \mathbf{x}_1, \nabla \mathbf{x}_2, \cdots, \nabla \mathbf{x}_n\}$ of gradient vectors at uniformly distributed sample points along the circle $C_r(p)$ centered at p with radius r. To make the sample density independent of r, we sample $6r$ number of gradient vectors on $C_r(p)$. The gradient vector at a sample point is computed using linear interpolation [27] of gradient vectors at the four nearest pixels. The expected mean gradient vector $\boldsymbol{\mu}_e$ is computed as the vector mean of the gradient vectors at all pixels inside the circular disk representing the immediate smaller scale, i.e., $2r - 1$. A constant 2-by-2 matrix is used for Σ_e, which is defined in terms of image noise. Image noise is represented by a covariance matrix Σ_N, which is computed over homogeneous regions. Assuming that noise is isotropic and uncorrelated, the matrix $\Sigma_N[1,1] = \Sigma_N[2,2] = \frac{\sigma^2}{2}$ and $\Sigma_N[1,2] = \Sigma_N[2,1] = 0$ is used, where σ^2 is the variance of the intensity gradients computed over homogenous regions. Finally, the covariance matrix Σ_e is defined as $\Sigma_e = 9\Sigma_N$.

Scale-based gradient at a pixel p is computed as the vector sum of the gradients over the circular disk $C_{I_s(p)/2}(p)$ centered at p, where $I_s(p)$ represents the computed blur-scale at p; note that blur-scale denotes the diameter of the local blur region, which is divided by two to get the value of radius. Our edge detection algorithm is applied on the scale-based gradient image, which is accomplished using the following steps similar to the algorithm by Canny [9] – (1) non-maximal suppression, (2) hysteresis, and (3) skeletonization[28, 29] and removing noisy branches[8, 30-32].

During non-maximal suppression, a pixel p with a blur-scale $2r$ is a local maxima if and only if there is no point q on the diameter of $C_r(p)$ along the gradient direction of p such that the scale-based gradient at q is greater than that of p. In the next step, hysteresis thresholding is applied using two threshold values t_{low} and t_{high} to select meaningful edge segments, while suppressing noisy edges. [9] The use of two thresholds allows to apply a high threshold value t_{high} for isolated noisy edge points and a low threshold value t_{low} for edge segments containing contextual information. Finally, the edge map obtained after hysteresis is skeletonized and noisy branches are pruned to get single pixel-thick edges.

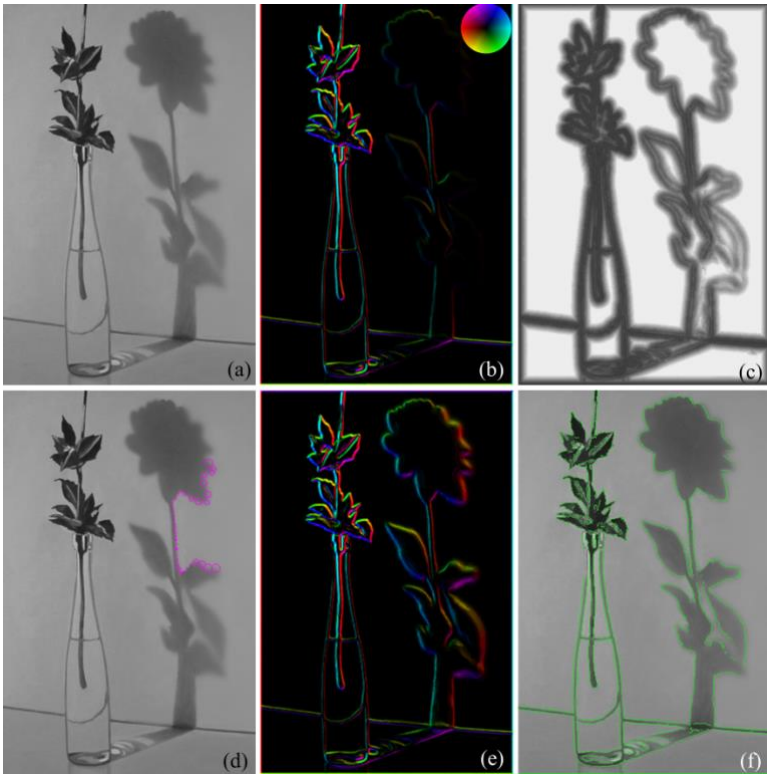

Fig. 1. Results of application of the new blur-scale computation and edge detection algorithms. (a) A grayscale image. (b) Color-coded representation of non-scale based gradient computation results using a constant DoG kernel. The color-coding scheme follows the color-disk, where the hue and intensity components of color represent the gradient orientation and magnitude, respectively. (c) Results of local blur-scale computation. (d) Illustration of blur-scales using circles centered at manually selected pixels along different edges. Diameters of individual circles represent blur-scales at respective pixels. (e) Color-coded display of scale-based gradient computation results using the same color-coding shown in (b). (f) Results of edge detection using blur-scale based gradients. Edge locations are shown in green.

3 Experiments and Results

In this section, we will discuss our experiments and results using the new blur-scale computation and edge detection algorithms. The algorithms are applied on both real and computer generated phantom images. For all experiments, a constant value of 0.002 was used for both c_1 and c_2 to ensure that, for the test criterion $\lambda_1(X_o|\boldsymbol{\mu}_e, \Sigma_e) > c_1$, at least three observed gradients have a Mahalanobis distance of two from their expected mean.

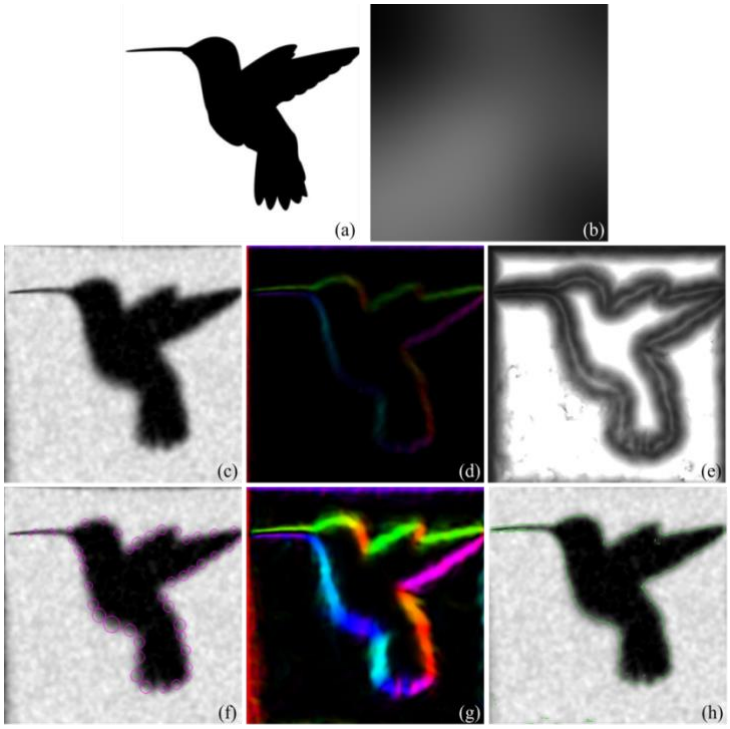

Fig. 2. Results of the new blur-scale computation and edge detection algorithms for a computer-generated phantom image. (a) Original binary image. (b) A slow varying computer-generated blur field used to apply a space-varying blur on the binary image. (c) Test phantom, generated by applying the blur field of (b) and a correlated white Gaussian noise at a contrast-to-noise ratio of 12 on (a). (d-h) same as Fig. 1(b-f) but for the phantom image shown in (c).

Results of blur-scale computation and edge detection for a grayscale image are shown in Fig. 1. Figure (a) shows a grayscale image of a plant and its shadow, and (b) represents the result of non-scale based gradient computation using a location invariant DoG kernel. Figure (c) presents the result of the blur-scale computation, where the intensity brightness is proportional to the local blur-scale. It may be noted from the blur-scale image that blur-scales along the shadow boundary form ridges that represent optimal edge locations. Also, the ridges along the shadow boundary are

brighter than the ridges along the sharp edges of the plant, which implies that blur-scales along the boundary of the shadow are higher as compared to blur-scales along the boundary of the plant. Finally, it is worthy to note that blur-scales at homogeneous regions far from an edge are large. In figure (d), computed blur-scales along different boundary regions are shown by circles centered at manually selected pixels along edges. Specifically, the diameter of each circle represents the value of the blur-scale at its center. It may be visually noted that individual circles fully cover local object interface transition-widths at respective locations. Also, along the shadow boundary, circles are larger indicating greater blur. The result of blur-scale based gradient computation is presented in figure (e). Following our algorithm, the computed blur-scale based gradient captures the total intensity difference across the full width of the object transition, which is visually notable along blurred regions of the shadow boundary. In general, gradient values at blurred locations on the shadow boundary are enhanced, while those near the sharp edges remain unchanged. This improvement in gradient computation will be helpful for precise detection of edges near highly blurred regions. In figure (f), edges detected by our blur-scale based edge detection algorithm are shown in green. It is encouraging to note that the sharp edges along the plant as well as blurred edges along the shadow boundary are fully recovered.

Fig. 2 presents the performance of our edge detection algorithm on a computer-generated noisy phantom. A phantom was generated from a binary image of a bird, shown in Fig. 2(a). A slow-varying blur field, as shown in (b), was applied on the binary phantom image in the form of Gaussian smoothing to generate a blurred grayscale image. This blurred image was further degenerated by a correlated white Gaussian noise at the contrast-to-noise ratio of 12 to get the final test phantom image shown in (c). Results of local gradient and blur-scale computation on the phantom image of (c) are presented in (d,e), respectively. An illustration of the local blur-scale values using circles at quasi-regular sample points along the object boundary is presented in (f). The displayed blur-scales in (f) are satisfactory with visual blur at individual edge locations. Finally, the result of blur-scale based gradient computation is shown in (g), which is displayed using the exact same color coding used for (d). The blur-scale based gradient successfully captures the slow-varying edges, which are hardly visible in the non-scale based gradient image in (d). Figure (h) shows the detected edges in green which is completely aligned to the boundary of the test phantom despite such high noise.

4 Conclusions

A new theory and algorithms for local blur-scale computation have been presented and their applications to edge-detection have been demonstrated. The performance of the new algorithms on both natural and phantom images has been examined and the results are presented. New statistical test criteria examining whether a set of observed gradient vectors follow an expected Gaussian distribution with a non-zero mean have been introduced and applied to compute blur-scale at individual image pixels. It has been experimentally observed that blur-scales capture the extent of blur along the

object boundary. Computed blur-scales have been applied to develop a scale-based gradient computation algorithm, where the gradient vectors over the local blur-scale region are summed. Results of scale-based gradient computation provide effective edge detection by enhancing gradient magnitudes along the blurred edges, while gradients at the sharp edges remain unchanged and noise in homogenous regions is suppressed. Also, computed blur-scale has been used to formulate a scale-based non-maxima suppression algorithm for edge detection. It has been experimentally shown that the new blur-scale based edge detection algorithm successfully detects edges even at blurred object regions. In the phantom experiment, it has been demonstrated that, despite the presence of significant noise and blur in the image, the algorithm successfully detects the boundary of the image. These initial results of blur-scale computation and edge detection are encouraging, which validates our new theory and algorithms for blur-scale computation and its applications.

References

1. Sonka, M., Hlavac, V., Boyle, R.: Image Processing, Analysis, and Machine Vision. Cengage Learning (2014)
2. Udupa, J.K., Herman, G.T.: 3D Imaging in Medicine. CRC Press, Boca Raton, FL (1991)
3. Müller, R., Van Campenhout, H., Van Damme, B., Van der Perre, G., Dequeker, J., Hildebrand, T., Rüegsegger, P.: Morphometric analysis of human bone biopsies: a quantitative structural comparison of histological sections and micro-computed tomography. Bone 23, 59-66 (1998)
4. Saetta, M., Di Stefano, A., Rosina, C., Thiene, G., Fabbri, L.M.: Quantitative structural analysis of peripheral airways and arteries in sudden fatal asthma. American Review of Respiratory Disease 143, 138-143 (1991)
5. Saha, P.K., Gomberg, B.R., Wehrli, F.W.: Three-dimensional digital topological characterization of cancellous bone architecture. International Journal of Imaging Systems and Technology 11, 81-90 (2000)
6. Chen, C., Zhang, X., Guo, J., Jin, D., Letuchy, E.M., Burns, T.L., Levy, S.M., Hoffman, E.A., Saha, P.K.: Quantitative imaging of peripheral trabecular bone microarchitecture using MDCT. Medical Physics 45, 236-249 (2018)
7. Chang, G., Rajapakse, C.S., Chen, C., Welbeck, A., Egol, K., Regatte, R.R., Saha, P.K., Honig, S.: 3-T MR Imaging of proximal femur microarchitecture in subjects with and without fragility fracture and nonosteoporotic proximal femur bone mineral density. Radiology 287, 608-619 (2018)
8. Saha, P.K., Xu, Y., Duan, H., Heiner, A., Liang, G.: Volumetric topological analysis: a novel approach for trabecular bone classification on the continuum between plates and rods. IEEE Trans. on Medical Imaging 29, 1821-1838 (2010)
9. Canny, J.: A computational approach to edge detection. IEEE Trans. on Pattern Analysis and Machine Intelligence 679-698 (1986)
10. Elder, J.H., Zucker, S.W.: Local scale control for edge detection and blur estimation. IEEE Trans. on Pattern Analysis and Machine Intelligence 20, 699-716 (1998)
11. Saha, P.K., Udupa, J.K.: Optimum image thresholding via class uncertainty and region homogeneity. IEEE Trans. on Pattern Analysis and Machine Intelligence 689-706 (2001)
12. Marr, D., Hildretch, E.: Theory of edge detection. Proceedings of Royal Society London B-207, 187-217 (1980)

13. Kass, M., Witkin, A., Terzopoulos, D.: Snakes: Active contour models. International Journal of Computer Vision 1, 321-331 (1988)
14. Otsu, N.: A threshold selection method from gray-level histograms. IEEE Trans. on Systems, Man, and Cybernetics 9, 62-66 (1979)
15. Saha, P.K., Udupa, J.K., Odhner, D.: Scale-based fuzzy connected image segmentation: theory, algorithms, and validation. Computer Vision and Image Understanding 77, 145-174 (2000)
16. Saha, P.K., Strand, R., Borgefors, G.: Digital topology and geometry in medical imaging: a survey. IEEE Trans. on Medical Imaging 34, 1940-1964 (2015)
17. Strand, R., Ciesielski, K.C., Malmberg, F., Saha, P.K.: The minimum barrier distance. Computer Vision and Image Understanding 117, 429-437 (2013)
18. Udupa, J.K., Saha, P.K.: Fuzzy connectedness and image segmentation. Proceedings of the IEEE 91, 1649-1669 (2003)
19. Udupa, J.K., Saha, P.K., Lotufo, R.d.A.: Relative fuzzy connectedness and object definition: theory, algorithms, and applications in image segmentation. IEEE Trans. on Pattern Analysis and Machine Intelligence 24, I-1500 (2002)
20. Saha, P.K., Udupa, J.K.: Iterative relative fuzzy connectedness and object definition: theory, algorithms, and applications in image segmentation. Proc. IEEE Workshop on Mathematical Methods in Biomedical Image Analysis, pp. 28-35. IEEE (2000)
21. Bao, P., Zhang, L., Wu, X.: Canny edge detection enhancement by scale multiplication. IEEE Trans. on Pattern Analysis and Machine Intelligence 27, 1485-1490 (2005)
22. Bergholm, F.: Edge focusing. IEEE Trans. on Pattern Analysis and Machine Intelligence 726-741 (1987)
23. Jeong, H., Kim, C.: Adaptive determination of filter scales for edge detection. IEEE Trans. on Pattern Analysis and Machine Intelligence 579-585 (1992)
24. Lindeberg, T.: Edge detection and ridge detection with automatic scale selection. International Journal of Computer Vision 30, 117-156 (1998)
25. Casella, G., Berger, R.L.: Statistical inference. Duxbury Pacific Grove, CA (2002)
26. Mahalanobis, P.C.: On the generalized distance in statistics. National Institute of Science of India (1936)
27. Meijering, E.H., Niessen, W.J., Viergever, M.A.: Quantitative evaluation of convolution-based methods for medical image interpolation. Medical Image Analysis 5, 111-126 (2001)
28. Saha, P.K., Borgefors, G., Sanniti di Baja, G.: A survey on skeletonization algorithms and their applications. Pattern Recognition Letters 76, 3-12 (2016)
29. Saha, P.K., Chaudhuri, B.B.: Detection of 3-D simple points for topology preserving transformations with application to thinning. IEEE Trans. on Pattern Analysis and Machine Intelligence 16, 1028-1032 (1994)
30. Németh, G., Kardos, P., Palágyi, K.: Thinning combined with iteration-by-iteration smoothing for 3D binary images. Graphical Models 73, 335-345 (2011)
31. Borgefors, G., Ramella, G., Sanniti di Baja, G.: Hierarchical decomposition of multiscale skeletons. IEEE Trans. on Pattern Analysis and Machine Intelligence 1296-1312 (2001)
32. Attali, D., Sanniti di Baja, G., Thiel, E.: Skeleton simplification through non significant branch removal. Image Processing and Communications 3, 63-72 (1997)